PHYSICAL REVIEW D **96,** 102003 (2017)

BICEP2 / *Keck Array* IX: New bounds on anisotropies of CMB polarization rotation and implications for axionlike particles and primordial magnetic fields

P. A. R. Ade,[1] Z. Ahmed,[2,3] R. W. Aikin,[4] K. D. Alexander,[5] D. Barkats,[5] S. J. Benton,[6] C. A. Bischoff,[7] J. J. Bock,[4,8] R. Bowens-Rubin,[5] J. A. Brevik,[4] I. Buder,[5] E. Bullock,[9] V. Buza,[5,10] J. Connors,[5] B. P. Crill,[8] L. Duband,[11] C. Dvorkin,[10] J. P. Filippini,[4,12] S. Fliescher,[13] T. St. Germaine,[10] T. Ghosh,[4] J. Grayson,[3] S. Harrison,[5] S. R. Hildebrandt,[4,8] G. C. Hilton,[14] H. Hui,[4] K. D. Irwin,[3,2,14] J. Kang,[3,2] K. S. Karkare,[5] E. Karpel,[3] J. P. Kaufman,[15] B. G. Keating,[15] S. Kefeli,[4] S. A. Kernasovskiy,[3] J. M. Kovac,[5,10] C. L. Kuo,[3,2] N. Larson,[16] E. M. Leitch,[17] K. G. Megerian,[8] L. Moncelsi,[4] T. Namikawa,[3,2,*] C. B. Netterfield,[6,18] H. T. Nguyen,[8] R. O'Brient,[4,8] R. W. Ogburn IV,[3,2] C. Pryke,[13,9] S. Richter,[5] A. Schillaci,[4] R. Schwarz,[13] C. D. Sheehy,[19] Z. K. Staniszewski,[4,8] B. Steinbach,[4] R. V. Sudiwala,[1] G. P. Teply,[15] K. L. Thompson,[3,2] J. E. Tolan,[3] C. Tucker,[1] A. D. Turner,[8] A. G. Vieregg,[5,16,17] A. C. Weber,[8] D. V. Wiebe,[20] J. Willmert,[13] C. L. Wong,[5,10] W. L. K. Wu,[3,21] and K. W. Yoon[3,2]

(*Keck Array* and BICEP2 Collaborations)

[1]*School of Physics and Astronomy, Cardiff University, Cardiff CF24 3AA, United Kingdom*
[2]*Kavli Institute for Particle Astrophysics and Cosmology, SLAC National Accelerator Laboratory, 2575 Sand Hill Rd, Menlo Park, California 94025, USA*
[3]*Department of Physics, Stanford University, Stanford, California 94305, USA*
[4]*Department of Physics, California Institute of Technology, Pasadena, California 91125, USA*
[5]*Harvard-Smithsonian Center for Astrophysics, 60 Garden Street MS 42, Cambridge, Massachusetts 02138, USA*
[6]*Department of Physics, University of Toronto, Toronto, Ontario M5S 1A7, Canada*
[7]*Department of Physics, University of Cincinnati, Cincinnati, Ohio 45221, USA*
[8]*Jet Propulsion Laboratory, Pasadena, California 91109, USA*
[9]*Minnesota Institute for Astrophysics, University of Minnesota, Minneapolis, Minnesota 55455, USA*
[10]*Department of Physics, Harvard University, Cambridge, Massachusetts 02138, USA*
[11]*Service des Basses Températures, Commissariat à l'Energie Atomique, 38054 Grenoble, France*
[12]*Department of Physics, University of Illinois at Urbana-Champaign, Urbana, Illinois 61801, USA*
[13]*School of Physics and Astronomy, University of Minnesota, Minneapolis, Minnesota 55455, USA*
[14]*National Institute of Standards and Technology, Boulder, Colorado 80305, USA*
[15]*Department of Physics, University of California, San Diego, La Jolla, California 92093, USA*
[16]*Department of Physics, Enrico Fermi Institute, University of Chicago, Chicago, Illinois 60637, USA*
[17]*Kavli Institute for Cosmological Physics, University of Chicago, Chicago, Illinois 60637, USA*
[18]*Canadian Institute for Advanced Research, Toronto, Ontario M5G 1Z8, Canada*
[19]*Brookhaven National Laboratory, Upton, New York 11973, USA*
[20]*Department of Physics and Astronomy, University of British Columbia, Vancouver, British Columbia V6T 1Z1, Canada*
[21]*Department of Physics, University of California, Berkeley, California 94720, USA*
(Received 13 May 2017; revised manuscript received 28 June 2017; published 9 November 2017)

We present the strongest constraints to date on anisotropies of cosmic microwave background (CMB) polarization rotation derived from 150 GHz data taken by the BICEP2 & *Keck Array* CMB experiments up to and including the 2014 observing season (BK14). The definition of the polarization angle in BK14 maps has gone through self-calibration in which the overall angle is adjusted to minimize the observed TB and EB power spectra. After this procedure, the QU maps lose sensitivity to a uniform polarization rotation but are still sensitive to anisotropies of polarization rotation. This analysis places constraints on the anisotropies of polarization rotation, which could be generated by CMB photons interacting with axionlike pseudoscalar fields or Faraday rotation induced by primordial magnetic fields. The sensitivity of BK14 maps (~ 3 μK-arc min) makes it possible to reconstruct anisotropies of the polarization rotation angle and measure their angular power spectrum much more precisely than previous attempts. Our data are found to be consistent with no polarization rotation anisotropies, improving the upper bound on the amplitude of the rotation angle spectrum by roughly an order of magnitude compared to the previous best constraints.

*Corresponding author.
toshiyan@stanford.edu

Our results lead to an order of magnitude better constraint on the coupling constant of the Chern-Simons electromagnetic term $g_{a\gamma} \leq 7.2 \times 10^{-2}/H_I$ (95% confidence) than the constraint derived from the B-mode spectrum, where H_I is the inflationary Hubble scale. This constraint leads to a limit on the decay constant of $10^{-6} \lesssim f_a/M_{\rm pl}$ at mass range of $10^{-33} \leq m_a \leq 10^{-28}$ eV for $r = 0.01$, assuming $g_{a\gamma} \sim \alpha/(2\pi f_a)$ with α denoting the fine structure constant. The upper bound on the amplitude of the primordial magnetic fields is 30 nG (95% confidence) from the polarization rotation anisotropies.

DOI: 10.1103/PhysRevD.96.102003

I. INTRODUCTION

The BICEP/*Keck Array* (BK) program has been making deep observations of cosmic microwave background (CMB) polarization at the South Pole. The 150 GHz data taken through 2014 (BK14) have been used to constrain primordial gravitational waves (GWs) to $r < 0.07$ (95% confidence, including Planck and WMAP) [1] and to detect gravitational lensing with high significance [2].

In addition to GWs and lensing, CMB polarization can also be used to test various theories of physics beyond the Standard Model. Measurements of the polarization rotation angle are known to be a unique probe of new physics containing pseudoscalar fields coupled with photons through the Chern-Simons term [3–9]:

$$\mathcal{L} \supset \frac{g_{a\gamma} a}{4} F_{\mu\nu} \tilde{F}^{\mu\nu}. \quad (1)$$

Here, a is a pseudoscalar field, $g_{a\gamma}$ is corresponding coupling constant, $F_{\mu\nu}$ is the electromagnetic field, and $\tilde{F}^{\mu\nu}$ is the dual of $F^{\mu\nu}$ (for review, see, e.g., Ref. [10] and references therein). The existence of the above pseudoscalar fields, also known as axionlike particles, is a generic prediction of string theory, and detection or any constraints on these fields can provide valuable implications for fundamental physics. The presence of the above pseudoscalar fields leads to cosmic birefringence, in which the CMB polarization angle is rotated by

$$\alpha = \frac{\Delta a g_{a\gamma}}{2}, \quad (2)$$

where Δa is the change of the pseudoscalar fields along the photons' trajectory between the observer and recombination (e.g., Ref. [6]). Fluctuations in Δa, as some models predict, lead to spatial variations in α (e.g., Refs. [8,11–13]). If the pseudoscalar field is effectively massless during inflation, the power spectrum of the fluctuations of the pseudoscalar field has a scale-invariant spectrum. Reference [8] shows that the power spectrum of α induced by these fluctuations is given as

$$\sqrt{\frac{L(L+1)C_L^{\alpha\alpha}}{2\pi}} = \frac{H_I g_{a\gamma}}{4\pi}, \quad (3)$$

in the large-scale limit ($L \lesssim 100$). Here, H_I is the inflationary Hubble parameter. Henceforth, we use L for the multipoles of α and ℓ for the CMB E and B modes.

The measurements of the rotation angle can also be used to probe primordial magnetic fields (PMFs) through the Faraday rotation of CMB polarization [14,15]. In the large-scale limit ($L \lesssim 100$), nearly scale-invariant PMFs lead to [16,17]

$$\sqrt{\frac{L(L+1)C_L^{\alpha\alpha}}{2\pi}} = 1.9 \times 10^{-4} \left(\frac{\nu}{150\,\mathrm{GHz}}\right)^{-2} \left(\frac{B_{1\,\mathrm{Mpc}}}{1\,\mathrm{nG}}\right). \quad (4)$$

The rotation angle from PMFs depends on the observing frequency. Compared to the BK14 150 GHz data, the BK14 95 GHz data have larger noise and lower angular resolution, and the 150 GHz data from BK14 place the strongest constraints on PMFs. Thus, we use the 150 GHz data in the following analysis. If we were to detect a rotation signal, then we would look for the same signal at 95 GHz to test whether it has the correct wavelength dependence for Faraday rotation.

The polarization rotation effect modifies the pattern of the CMB polarization map and leads to mixing of E and B modes. Since E modes at last scattering are much brighter than the B mode, this effect is mostly characterized by leakage from E to B modes. The rotation-induced B mode is proportional to αE, so the rotation angle may be measured from the correlation of E and B modes. Because temperature is correlated with E modes, the rotation angle may also be measured from temperature-B correlation. These effects are the same for any sources of the rotation. Using EB and/or temperature-B correlations, the uniform polarization rotation angle has been constrained by several groups including WMAP [18], BICEP1 [19], and Planck [20] (see also Refs. [21,22]). The current best constraints are limited by the accuracy of absolute detector polarization angle calibration.

Inhomogeneities in pseudoscalar fields and/or PMFs produce anisotropies of the rotation angle [8,17,23]. If the polarization angle is anisotropic, the correlation between E and rotation-induced B modes determined at each small patch is also anisotropic. In Fourier space, different Fourier modes of E and B modes correlate. Thus, the anisotropy of the polarization rotation is extracted through the mode coupling between E and B modes.

The angular power spectrum of the extracted anisotropic rotation is the four-point correlation of E and B modes and can be reconstructed from the $EBEB$ trispectrum measurement [24]. Compared to a uniform rotation, measurements of the anisotropic rotation angle are insensitive to the accuracy of the overall rotation angle. There already exist constraints on the cosmic birefringence anisotropies from the CMB. Reference [12] presents constraints on anisotropies of the cosmic birefringence using the $TBTB$ trispectrum of WMAP7 data, while Refs. [25–30] used two-point correlation. The most stringent constraints prior to this paper were published by POLARBEAR [31].

In this paper, we use a similar method to improve constraints on the rotation anisotropies using polarization maps made by BK.

II. DATA AND SIMULATIONS

We use the same data set described in Refs. [1,2]: BICEP/ *Keck Array* maps which coadd all data taken up to and including the 2014 observing season—we refer to these as the BK14 maps. In this work, we use the 150 GHz Q/U maps. These have a depth of 3.0 μK-arc min over an effective area of $\sim$395 deg^2, centered on RA 0h, Dec. −57.5 deg.

We reuse the standard sets of simulations described in Ref. [1] and previous papers: lensed CMB signal-only simulations [denoted by "lensed-Lambda Cold-Dark-Matter (ΛCDM)"] with input lensed maps generated by LensPix [32], instrumental noise, and dust foreground, each having 499 realizations. The details of the CMB signal and noise simulations are given in Sec. V of Ref. [33], and the dust simulations are described in Sec. IV A of Ref. [34] and Appendix E of Ref. [1]. In addition, we also generate random fields of anisotropic rotation maps, $\alpha(\hat{\boldsymbol{n}})$, on the full sky (where $\hat{\boldsymbol{n}}$ denotes a position on the sphere) of which the power spectrum is described by

$$\frac{L(L+1)}{2\pi}C_L^{\alpha\alpha} = A_{CB}\times 10^{-4}\ [\mathrm{rad}^2], \tag{5}$$

with varying A_{CB}. Since previous constraints on the cosmic birefringence anisotropies are derived based on this spectrum, our result can be directly compared with the previous studies (see, e.g., Refs. [8,12,31]).

The simulated full-sky CMB maps are rotated by $\alpha(\hat{\boldsymbol{n}})$ before beam smoothing according to

$$[Q' \pm \mathrm{i}U'](\hat{\boldsymbol{n}}) = \mathrm{e}^{\pm 2\mathrm{i}\alpha(\hat{\boldsymbol{n}})}[Q \pm \mathrm{i}U](\hat{\boldsymbol{n}}). \tag{6}$$

As described in Ref. [35], we simulate observed maps by multiplying the BK14 observing matrix with the rotated maps. We denote these maps as "rotated-ΛCDM" simulations. The rotated-ΛCDM, instrumental noise, and dust simulated maps are then combined to estimate the transfer function, mean-field bias, disconnected bias, and the uncertainties of the power spectrum of reconstructed α. The reconstructed rotation power can then be compared against lensed-ΛCDM simulations under the null hypothesis to evaluate statistical uncertainties.

To properly include cosmic variance from α, rotated-ΛCDM simulations must be used. To our knowledge, this has not been done in previous papers, in which unrotated simulations are used to calculate uncertainties [12,31]). In this paper, we present the test of the null hypothesis using the lensed-ΛCDM simulations to compare our measurements with prior attempts and also show constraints on the anisotropic polarization rotation with the rotated-ΛCDM simulations.

III. ANALYSIS

The rotation angle anisotropies can be reconstructed from the off-diagonal mode-mode covariance within, and between, the E and B modes. An estimator of $\alpha(\hat{\boldsymbol{n}})$ has a quadratic form similar to the lensing estimator [24,36]. The power spectrum of the anisotropic rotation angle $C_L^{\alpha\alpha}$ can be obtained by squaring the rotation estimator. Here, we describe the method used to reconstruct the anisotropic rotation angle from the BK14 polarization maps, to calculate the rotation spectrum, and to evaluate the amplitudes of the resulting spectra. The details and verification of our analysis method are described in Ref. [37].

Under the flat-sky approximation, the CMB E and B modes are given by

$$E_\ell \pm iB_\ell = -\int \mathrm{d}^2\hat{\boldsymbol{n}}\mathrm{e}^{-\mathrm{i}\hat{\boldsymbol{n}}\cdot\boldsymbol{\ell}}[Q \pm \mathrm{i}U](\hat{\boldsymbol{n}})\mathrm{e}^{\mp 2\mathrm{i}\varphi_\ell}, \tag{7}$$

where φ_ℓ is the angle of $\boldsymbol{\ell}$ measured from the Stokes Q axis. From Eq. (6), the rotated CMB E and B modes are given by [24]

$$E'_\ell = E_\ell + \int \frac{\mathrm{d}^2\boldsymbol{L}}{(2\pi)^2}2\alpha_{\boldsymbol{L}} \times [E_{\boldsymbol{\ell}-\boldsymbol{L}}\cos 2(\varphi_{\boldsymbol{\ell}-\boldsymbol{L}} - \varphi_\ell) + B_{\boldsymbol{\ell}-\boldsymbol{L}}\sin 2(\varphi_{\boldsymbol{\ell}-\boldsymbol{L}} - \varphi_\ell)] \tag{8}$$

$$B'_\ell = B_\ell + \int \frac{\mathrm{d}^2\boldsymbol{L}}{(2\pi)^2}2\alpha_{\boldsymbol{L}} \times [E_{\boldsymbol{\ell}-\boldsymbol{L}}\sin 2(\varphi_{\boldsymbol{\ell}-\boldsymbol{L}} - \varphi_\ell) - B_{\boldsymbol{\ell}-\boldsymbol{L}}\cos 2(\varphi_{\boldsymbol{\ell}-\boldsymbol{L}} - \varphi_\ell)]. \tag{9}$$

Up to first order in the anisotropic part of α, the rotation-induced off-diagonal elements of the covariance are [24]

$$\langle E'_\ell B'_{\boldsymbol{L}-\boldsymbol{\ell}}\rangle_{\mathrm{CMB}} = w^{\alpha}_{\boldsymbol{L},\boldsymbol{\ell}}\alpha_{\boldsymbol{L}}, \tag{10}$$

where $\langle\cdots\rangle_{\mathrm{CMB}}$ denotes the ensemble average with a fixed realization of α and the weight function is

$$w^{\alpha}_{\boldsymbol{L},\ell} = 2\tilde{C}^{\rm EE}_{\ell} \cos 2(\varphi_{\ell} - \varphi_{\boldsymbol{L}-\ell}), \tag{11}$$

where $\tilde{C}^{\rm EE}_{\ell}$ is the lensed E-mode power spectrum. The term originating from the lensing B mode is ignored since the improvement of the sensitivity to the polarization rotation anisotropies by the inclusion of this term is negligible [31]. Similar to the lensing reconstruction, the quadratic estimator of α is constructed as a convolution of the E and B modes with the weight function of Eq. (11) [24]. The only difference between the reconstruction of α and the lensing potential, ϕ, is the weight function. Similar to the lensing analysis, we use E and B modes obtained from the matrix-based $E-B$ separation technique as described in Ref. [35] to avoid E-to-B leakage.

From the reconstructed α, the rotation spectrum is estimated in the same way as the lensing spectrum shown in Ref. [2]. The disconnected bias is estimated with the realization-dependent method [37], which is more accurate than simulation-based subtraction [38] and also mitigates the off-diagonal elements of covariance [39].

To quantify the constraints on polarization rotation anisotropies, we estimate the amplitude for the reconstructed rotation spectrum [2]

$$\hat{A}_{CB} = \frac{\sum_b w_b A_b}{\sum_b w_b}, \tag{12}$$

where $A_b = C_b/C^{\rm fid}_b$ is an amplitude relative to a fiducial power spectrum at each multipole bin, b. The coefficients w_b are defined as

$$w_b = \sum_{b'} C^{\rm fid}_b \mathbf{Cov}^{-1}_{bb'} C^{\rm fid}_{b'}, \tag{13}$$

and the power spectrum covariance $\mathbf{Cov}_{bb'}$ is estimated from the lensed- and rotated-ΛCDM + noise + dust simulations for evaluating the null hypothesis and constraining $A_{\rm CB}$, respectively. The fiducial rotation spectrum $C^{\rm fid}_b$ corresponds to $A_{\rm CB} = 1$.

In the reconstruction from the rotated-ΛCDM simulations, even after the subtraction of a disconnected bias, there exists a non-negligible correction from the secondary contraction at smaller scales [37]. As detailed in Ref. [37], the secondary contraction of the *EBEB* trispectrum (N1 term) is proportional to the signal, so we include this term for estimating $\hat{A}_{\rm CB}$. On the other hand, the lensing-induced trispectrum is negligibly small for BK14 data [37].

IV. RECONSTRUCTED SPECTRUM

Figure 1 shows the power spectrum of the reconstructed rotation angle from BK14 data. In the baseline analysis, we use CMB multipoles between $\ell = 30$ and 700 but remove B modes for multipoles $\ell < 150$, which significantly reduces the large-scale dust foreground contamination (see Ref. [2]). In addition to the baseline analysis, we also show the cases with different choices of CMB multipole ranges used for the rotation angle reconstruction and the case without a dust component. We calculate the χ^2 probability to exceed (PTE) for the baseline analysis and each variant analysis against the null hypothesis. For the baseline case, the χ^2 PTE is found to be 0.25. The χ^2 PTEs for other cases are in the range between 0.18 and 0.59. These results indicate that the reconstructed spectrum is consistent with the null hypothesis irrespective of the choice of the multipole range and the inclusion of dust in the simulations. Figure 1 indicates that, to constrain the model of Eq. (5), the largest-scale multipole bin is the most important. One advantage of BK14 data is the capability of measuring such large scales.

Figure 2 shows the histogram of $\hat{A}_{\rm CB}$ for each realization of the null (lensed ΛCDM + noise + dust) simulations. The observed $\hat{A}_{\rm CB}$ is shown as the vertical solid line and is consistent with the null hypothesis. The rotation spectrum amplitude is estimated from Eq. (12). We also show the histogram obtained from the POLARBEAR analysis [40], which leads to $A_{\rm CB} < 3.1$ at 95% confidence (ignoring the cosmic variance from α). The statistical uncertainties for BK14 are an order of magnitude smaller. The histogram obtained in this work is skewed because the constraint on $A_{\rm CB}$ is mostly determined by the largest-scale multipoles where the PDF of the power spectrum becomes a chi-squared distribution.

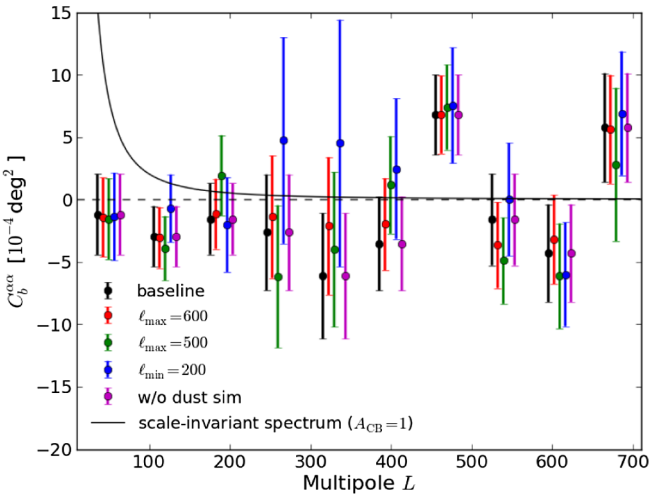

FIG. 1. Angular power spectrum of rotation anisotropies measured from BK14 real data using the standard lensed-ΛCDM + noise + dust simulation to obtain the power spectrum and uncertainties. In addition to the baseline analysis, we also show cases with different choices of the CMB multipole range used for the rotation angle reconstruction and a case without the inclusion of the dust simulation. We group the multipoles up to 700 into 10 bins. The solid line shows the scale-invariant spectrum of Eq. (5) with $A_{\rm CB} = 1$.

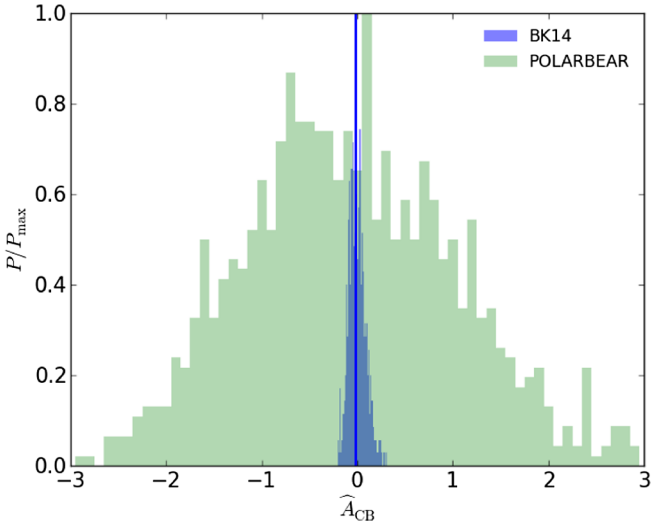

FIG. 2. Histogram of rotation spectrum amplitude $\hat{A}_{\rm CB}$ from BK14 data. The blue histogram shows the results from the standard ΛCDM simulations, while the green histogram shows the POLARBEAR result [40]. The blue vertical line shows the value from the observed spectrum.

V. COSMOLOGICAL IMPLICATIONS

To obtain a constraint on $A_{\rm CB}$, we next apply the direct likelihood method of Ref. [41] to $A_{\rm CB}$. We run simulations with a varying overall amplitude of the input scale-invariant spectrum up to $A_{\rm CB} = 1.5$ to obtain the distribution of $\hat{A}_{\rm CB}$ for each value of the input $A_{\rm CB}$. The posterior distribution for the amplitude parameter $A_{\rm CB}$ is obtained from this direct likelihood by assuming a flat prior on $A_{\rm CB}$ for $A_{\rm CB} \leq 1.5$. The resulting constraint is $A_{\rm CB} \leq 0.33$ at 95% confidence and is the best constraint on cosmic birefringence anisotropies to date.

Using Eq. (3), this $A_{\rm CB}$ constraint can be translated into constraints on coupling between axionlike particles and photons,

$$g_{a\gamma} \leq \frac{7.2 \times 10^{-2}}{H_I}. \tag{14}$$

This is at least an order of magnitude better than the constraint from Ref. [6], which obtains $g_{a\gamma} H_I \lesssim 1$.

The constraint above leads to implications for axionlike particles with a small mass as discussed in, e.g., Ref. [10]. In general, if axionlike particles have a mass, m_a, the field value perturbation starts to oscillate when the Hubble friction becomes inefficient as similar to the uniform value. The change of the field value in Eq. (2), and equivalently the polarization rotation angle, is significantly suppressed after the oscillation. Thus, the polarization rotation anisotropies are generated if the oscillation of the axionlike particles starts after recombination ($t = t_{\rm rec}$). Since the time of the transition to oscillation is given by $H(t_{\rm osc}) \sim m_a$, the mass range of the axionlike particles is $m_a = 10^{-33} - 10^{-28}$ eV where the lower limit comes from $m_a \sim H_0$ and the upper bound comes from $m_a \sim H(t_{\rm rec})$. The string axion generally predicts such a mass spectrum. According to Fig. 2 of Ref. [42], the constraint on $g_{a\gamma}$ presented above is much tighter than other experiments at $m_a = 10^{-33} - 10^{-28}$ if the tensor-to-scalar ratio is $r \sim 0.01$.

The coupling constant is related to the decay constant f_a as $g_{a\gamma} = (\alpha/2\pi) C_{a\gamma}/f_a$ where α is the fine structure constant and $C_{a\gamma}$ is a model-dependent dimensionless coupling. The typical value of $C_{a\gamma}$ is $\mathcal{O}(1)$. The value of the decay constant in string theory models is typically $f_a \sim 10^{16}$ GeV (e.g., the model-independent axion in heterotic string theory and M-theory axiverse) but could be $f_a \lesssim M_{\rm pl}$ (type IIB theory) with $M_{\rm pl}$ denoting the Planck energy scale [10]. Our constraint tightens the allowed region of f_a for string axions with a mass within the above mass range. For example, if $r \sim 0.01$ and $C_{a\gamma} \sim 1$, we obtain $H_I \sim 10^{-5} M_{\rm pl}$, and the allowed range becomes $10^{-6} \lesssim f_a/M_{\rm pl} \lesssim 1$. In the near future, measurement of polarization rotation from CMB-S4[1] would further improve the lower bound by ∼4–5 orders of magnitude compared to our results, and significantly constrain f_a.

Following Refs. [17,31,43], we can also convert the above upper bound to the amplitude of the PMFs. The above result constrains the strength of the scale-invariant PMFs smoothed over 1 Mpc to $B_{1\ {\rm Mpc}} \leq 30$ nG, which is roughly three times better than that obtained from the previous best constraints on the polarization rotation (note that other statistics such as the POLARBEAR BB spectrum at high ℓ can further tighten the magnetic-field constraint compared to the trispectrum constraint presented here).

Note that a BB spectrum is also generated by the anisotropies of the cosmic birefringence through conversion from E to B modes. The BK14 BB spectrum is, however, less sensitive to cosmic polarization rotation anisotropies than $C_L^{\alpha\alpha}$, and the upper bound on the cosmic polarization rotation anisotropies using the BB spectrum is much larger than $A_{CB} \leq 0.33$. In other words, the results in this paper also rule out significant contributions from cosmic birefringence to BK14's main BB results, a possibility raised by Ref. [44].

VI. DISCUSSION

The BK14 data have been extensively searched for possible systematics in previous publications in the power spectrum and lensing trispectrum. To further test potential systematic contamination in the measured rotation spectrum, we perform rotation reconstruction on differenced ("jackknife") maps and check whether they are consistent with no polarization rotation (see Ref. [45] for the details of the jackknife maps). Table I shows the PTE of the χ^2 observed value constructed for these jackknife tests. The jackknife spectra show no evidence of spurious signals.

[1] https://cmb-s4.org/CMB-S4workshops/index.php/Main_Page.

TABLE I. Probability to exceed a χ^2 statistic for the jackknife tests (see Ref. [45] for definitions of these jackknife splits).

Deck	0.822
Scan direction	0.856
Tag split	0.064
Tile	0.285
Phase	0.776
Multiplexing column	0.383
Alternative deck	0.567
Multiplexing row	0.715
Tile/deck	0.964
Focal plane inner/outer	0.375
Tile top/bottom	0.924
Tile inner/outer	0.248
Moon	0.375
A/B offset best/worst	0.194

Galactic dust contamination affects the rotation spectrum measurement by producing an additional disconnected bias and trispectrum induced by dust non-Gaussianity. While a thorough estimation of these two effects requires a reliable non-Gaussian dust simulation, the following evidence demonstrates that our rotation spectrum measurement is not significantly affected by Galactic dust:

(i) We estimate the rotation spectrum by repeating the simulations with no dust and show that the change of the spectrum is negligible compared to the statistical uncertainties. This means that the additional disconnected bias by the Gaussian dust component is negligible. Since the power of the non-Gaussian dust is comparable to that of the Gaussian dust, the impact of the non-Gaussian dust on the disconnected bias would also be negligible.

(ii) To test the possible impact of dust, we tighten the cut on large-scale B modes from $150 < \ell$ to $200 < \ell$. The results remain consistent with the null hypothesis.

(iii) The dust could also lead to nonzero cross-power between the lensing and rotation maps. We cross-correlate the reconstructed rotation angle with the reconstructed lensing maps from BK14 shown in our lensing paper [2] and also with the public Planck 2015 lensing maps [46]. The χ^2 PTEs of these cross-spectra are 0.75 for $\alpha \times \kappa^{\mathrm{BK14}}$ and 0.63 for $\alpha \times \kappa^{\mathrm{P15}}$. We find the cross-spectrum to be consistent with zero.

These negative results suggest that the dust foreground contamination is not significant in the reconstructed rotation spectrum.

In our analysis, the overall polarization angle is calibrated by minimizing the TB and EB spectra [1,19,31,47]. However, limited accuracy of relative detector polarization calibration can also affect rotation spectrum measurements. To test this, we generate a set of signal-only time-ordered-data (TOD) simulations in which the baseline detector polarization angles are offset according to measured values for Keck 2014 data (see Ref. [48] for details). We then coadd them to maps using the nominal detector polarization angles. We repeat the analysis replacing the standard ΛCDM signal with this simulation, finding that the change in the reconstructed power spectrum is $<1\%$ of the 1σ statistical uncertainty in all band powers. Even if we repeat the analysis using the simulation in which the offsets from nominal are multiplied by 5, the change in the reconstructed spectrum is still $\sim 1\%$ of the 1σ statistical error. We therefore conclude that the systematic errors due to relative detector polarization angle offsets are negligible in our analysis.

VII. CONCLUSION

We present measurement of anisotropies of the CMB polarization rotation angle using BK14 data and find that the spectrum is in agreement with the null hypothesis (the standard ΛCDM prediction). The 95% upper bound on the amplitude of the scale-invariant rotation spectrum relevant to the inflationary scenario is $0.33 \times 10^{-4}\,[\mathrm{rad}^2] = 0.11\,\mathrm{deg}^2$, which is approximately ten times better than the best previous result [40]. The measured rotation spectrum is used to constrain cosmic birefringence from axionlike particles and Faraday rotation of PMFs. The constraint presented in this paper tightens the allowed range of the coupling constant for axionlike particles with $m_a = 10^{-33}$–10^{-28}. At this mass range, the CMB polarization rotation measurement is the best avenue to probe the axionlike particles, and in the near future, CMB-S4 will further tighten the allowed parameter space. We test systematics in the measured rotation spectrum by 1) performing jackknife null tests, 2) cross-correlating with gravitational lensing maps, and 3) evaluating the effect of relative rotation angle offsets between detectors, finding no spurious signals.

The anisotropic rotation angle is a unique probe of parity-violating models, and its measurement is important to test new physical theories of the early Universe. Future CMB experiments such as the BICEP Array, Advanced ACT, CMB-S4, LiteBIRD, Simons Array, and SPT-3G will measure rotation angle anisotropies more precisely.

ACKNOWLEDGMENTS

The *Keck Array* project has been made possible through support from the National Science Foundation under Grants No. ANT-1145172 (Harvard), No. ANT-1145143 (Minnesota), and& No. ANT-1145248 (Stanford) and from the Keck Foundation (Caltech). The development of antenna-coupled detector technology was supported by the JPL Research and Technology Development Fund and Grants No. 06-ARPA206-0040 and No. 10-SAT10-0017 from the NASA APRA and SAT programs. The development and testing of focal planes were supported by the Gordon and Betty Moore Foundation at Caltech. Readout electronics were supported by a Canada Foundation for

Innovation grant to UBC. The computations in this paper were run on the Odyssey cluster supported by the FAS Science Division Research Computing Grou p at Harvard University. The analysis effort at Stanford and SLAC is partially supported by the U.S. Department of Energy Office of Science. We thank the staff of the U.S. Antarctic Program and in particular the South Pole Station, without whose help this research would not have been possible. Most special thanks go to our heroic winter-overs Robert Schwarz and Steffen Richter. We thank all those who have contributed past efforts to the BICEP/*Keck Array* series of experiments, including the BICEP1 team. We thank Chang Feng for providing the histogram data shown in Ref. [31].

[1] BICEP2/*Keck Array* Collaboration VI, Phys. Rev. Lett. **116**, 031302 (2015).
[2] BICEP2/*Keck Array* Collaboration VIII, Astrophys. J. **833**, 228 (2016).
[3] W.-T. Ni, Phys. Rev. Lett. **38**, 301 (1977).
[4] S. M. Carroll, Phys. Rev. Lett. **81**, 3067 (1998).
[5] M. Li and X. Zhang, Phys. Rev. D **78**, 103516 (2008).
[6] M. Pospelov, A. Ritz, and C. Skordis, Phys. Rev. Lett. **103**, 051302 (2009).
[7] F. Finelli and M. Galaverni, Phys. Rev. D **79**, 063002 (2009).
[8] R. R. Caldwell, V. Gluscevic, and M. Kamionkowski, Phys. Rev. D **84**, 043504 (2011).
[9] G.-C. Liu and K.-W. Ng, Phys. Dark Universe **16**, 22 (2017).
[10] D. J. E. Marsh, Phys. Rep. **643**, 1 (2016).
[11] M. Kamionkowski, Phys. Rev. D **82**, 047302 (2010).
[12] V. Gluscevic, M. Kamionkowski, and D. Hanson, Phys. Rev. D **87**, 047303 (2013).
[13] D. Leon, J. Kaufman, B. Keating, and M. Mewes, Mod. Phys. Lett. A **32**, 1730002 (2017).
[14] A. Kosowsky and A. Loeb, Astrophys. J. **469**, 1 (1996).
[15] D. D. Harari, J. D. Hayward, and M. Zaldarriaga, Phys. Rev. D **55**, 1841 (1997).
[16] A. Yadav, L. Pogosian, and T. Vachaspati, Phys. Rev. D **86**, 123009 (2012).
[17] S. De, L. Pogosian, and T. Vachaspati, Phys. Rev. D **88**, 063527 (2013).
[18] G. Hinshaw *et al.* (WMAP Collaboration), Astrophys. J. **208**, 19 (2013).
[19] J. P. Kaufman, Phys. Rev. D **89**, 062006 (2014).
[20] Planck Collaboration, Astron. Astrophys. **596**, A13 (2016).
[21] A. Gruppuso, Int. J. Mod. Phys. D **25**, 1640007 (2016).
[22] C. R. Contaldi, Int. J. Mod. Phys. D **25**, 1640014 (2016).
[23] W. Zhao and M. Li, Phys. Rev. D **89**, 103518 (2014).
[24] M. Kamionkowski, Phys. Rev. Lett. **102**, 111302 (2009).
[25] A. Gruppuso, P. Natoli, N. Mandolesi, A. DeRosa, and F. Paci, J. Cosmol. Astropart. Phys. 02 (2012) 023.
[26] M. Li and B. Yu, J. Cosmol. Astropart. Phys. 06 (2013) 016.
[27] S. di Serego Alighieri, W.-T. Ni, and W.-P. Pan, Astrophys. J. **792**, 35 (2014).
[28] S.-Y. Li, J.-Q. Xia, M. Li, H. Li, and X. Zhang, Astrophys. J. **799**, 211 (2015).
[29] H.-H. Mei, W.-T. Ni, W.-P. Pan, L. Xu, and S. di Serego Alighieri, Astrophys. J. **805**, 107 (2015).
[30] W. P. Pan, S. di Serego Alighieri, W. T. Ni, and L. Xu (2017), p. 353, https://inspirehep.net/record/1435020/files/arXiv:1603.08193.pdf.
[31] POLARBEAR Collaboration, Phys. Rev. D **92**, 123509 (2015).
[32] A. Lewis, Phys. Rev. D **71**, 083008 (2005).
[33] BICEP2 Collaboration I, Phys. Rev. Lett. **112**, 241101 (2014).
[34] The BICEP2/Keck and Planck Collaborations, Phys. Rev. Lett. **114**, 101301 (2015).
[35] BICEP2/*Keck Array* Collaboration VII, Astrophys. J. **825**, 66 (2016).
[36] A. Yadav, R. Biswas, M. Su, and M. Zaldarriaga, Phys. Rev. D **79**, 123009 (2009).
[37] T. Namikawa, Phys. Rev. D **95**, 043523 (2017).
[38] T. Namikawa, D. Hanson, and R. Takahashi, Mon. Not. R. Astron. Soc. **431**, 609 (2013).
[39] D. Hanson, A. Challinor, G. Efstathiou, and P. Bielewicz, Phys. Rev. D **83**, 043005 (2011).
[40] C. Feng (private communication).
[41] D. Barkats *et al.*, Astrophys. J. **783**, 67 (2014).
[42] A. Ringwald (2014), p. 223, https://inspirehep.net/record/1304441/files/arXiv:1407.0546.pdf.
[43] L. Pogosian, Mon. Not. R. Astron. Soc. **438**, 2508 (2014).
[44] S.-Y. Li, J.-Q. Xia, M. Li, H. Li, and X. Zhang, Phys. Lett. B **751**, 579 (2015).
[45] BICEP2 Collaboration III, Astrophys. J. **814**, 110 (2015).
[46] Planck Collaboration, Astron. Astrophys. **594**, A15 (2016).
[47] B. Keating, M. Shimon, and A. Yadav, Astrophys. J. **762**, L23 (2013).
[48] BICEP2 Collaboration IV, Astrophys. J. **806**, 206 (2015).